Embedded density functional approach for calculations of adsorption on ionic crystals

Eugene V. Stefanovich[a] and Thanh N. Truong[b]
Department of Chemistry, University of Utah, Salt Lake City, Utah 84112

(Received 10 August 1995; accepted 17 November 1995)

We present an embedded density functional approach to study adsorption on crystalline surfaces. Following ideas suggested by Cortona, Wesolowski, and Warshel, we divide the total system into a quantum cluster and the surrounding lattice whose density is assumed to be the same as in the ideal crystal. In this case the Kohn–Sham Hamiltonian for electrons in the cluster contains additional terms corresponding to the Coulomb, exchange, correlation, and ''nonadditive kinetic energy'' potentials from the environment. Test calculations for the He and Ar dimers, $X-H_2O$ molecular complexes ($X=Li^+$, Na^+, K^+, F^- or Cl^-) and water adsorption on the (001) surface of the NaCl crystal suggest that this model provides a promising alternative for cluster models employed earlier for calculations of defects and adsorption on ionic crystals. © *1996 American Institute of Physics.* [S0021-9606(96)03208-6]

I. INTRODUCTION

Theoretical studies of chemical processes on the surfaces of solids are very important for further progress in such areas as adsorption, catalysis, microelectronics, and nanotechnology. The computational challenge is to find an adequate balance between local character of the chemical bonds in the adsorption complex and extended nature of electronic states in the substrate. Similar problems arise in studies of point defects in the bulk of crystals.

Presently, there are two main groups of quantum mechanical approaches for solution of these problems; the ''perturbed crystal'' method which uses the Green function formalism[1,2] and the embedded cluster method which uses the concept of ''perturbed cluster.''[3–6] In this paper, we will focus on the latter approach, which means that the system under study is divided into two parts: *cluster* (local region of the defect or adsorption site) and the crystalline *environment* (the rest of the crystal). The electronic structure of the cluster is computed using standard quantum chemistry methods taking into account an external potential generated by the environment.

The theoretical basis for majority of embedded cluster models lies in the concepts of group-function theory[7–9] which was formulated in the framework of the molecular orbital (MO) electronic structure theory. The total wave function of the system is approximated as an antisymmetrized product

$$\Psi=\hat{A}[\Psi_c\Psi_f], \tag{1}$$

where $\hat{A}$ is the antisymmetrization operator, Ψ_c is the wave function of the cluster, and Ψ_f is the wave function of the environment which should be found from separate periodic crystal calculations and kept fixed while Ψ_c is determined from a cluster Hamiltonian with external field produced by the environment. The embedded cluster method is usually applied to ionic crystals whose wave function can be well approximated as an antisymmetrized product of weakly overlapping spherical wave functions of individual closed shell ions. In this case the ions in the environment can be represented as whole-ion pseudopotentials (WIP) or model potentials.

In many practical embedded cluster calculations of defects in ionic crystals, cations are represented as effective core pseudopotentials (ECP) of the corresponding atom while anions are considered as point charges.[10–16] More accurate description of the cluster–lattice interaction can be achieved by optimizing embedding potentials for ions in crystal[17] and taking into account the long-range polarization of the environment by the cluster.[3,4,18]

The mathematical formulations of the above MO embedded cluster approach require a strong orthogonality condition between wave functions of different electronic groups and neglect the intergroup electron correlation. Although, such approximations can be removed in more sophisticated and general formulations (see Ref. 19 and references therein), the resulting theory is quite complicated and no practical implementation has yet been done.

Latest developments of the density functional theory (DFT) show that this computational method can compete with the MO based techniques in accuracy and efficiency. An advantage of the DFT methods is that the basic variable of the theory is the electron density $\rho(\mathbf{r})$ in the 3D coordinate space and exchange and correlation energies can be approximated with a high degree of accuracy by simple functionals of $\rho(\mathbf{r})$ and its gradient. These features of the DFT theory allow to calculate efficiently the Coulomb, exchange and correlation potentials acting on cluster electrons from the environment. However, the total embedding potential should also take into account the Pauli exclusion principle which effectively confines electrons inside the cluster. In earlier formulations of the DFT cluster method,[20–22] the latter effect was taken into account by using artificial methods such as

[a]On leave from the Institute of Chemical Physics, University of Latvia, 19 Rainis Blvd., Riga, LV 1586, Latvia.
[b]Author to whom correspondence should be addressed.

 0021-9606/96/104(8)/2946/10/$10.00

employing limited basis sets or adding repulsive potentials in the core regions of atoms surrounding the cluster. Cortona realized that this repulsive effect is closely related to the nonadditivity of the kinetic energy functional and added corresponding nonadditive kinetic energy potential to the clusterlike boundary conditions in his calculations of periodic crystals.[23–26] Wesolowski and Warshel modified Cortona's theory for applications to the solvation phenomena.[27,28] Below, we present the main ideas of Cortona's method (to be referred as embedded DFT method or EDFT) in the form suitable for studying adsorption on crystal surfaces which is the main goal of the present paper. The same approach can be used also for studying defects in the bulk. For more details and comparison of EDFT with other computational techniques, we refer readers to Cortona's report.[24]

II. EMBEDDED DENSITY FUNCTIONAL THEORY

Basic theorems of DFT state that ground state properties of any chemical system are determined unambiguously by the total electron density. Denote $\rho_{id}(\mathbf{r})$ as the electron density of the unperturbed (ideal) crystal surface, which can be found from periodic crystal calculations, and $\rho(\mathbf{r})$ the electron density of the surface with defect and/or adsorbate. In the absence of long range polarization effects we can assume that these two densities are different only inside a finite volume V (cluster) around the defect. Therefore, we can divide the total electron density into two parts,

$$\rho(\mathbf{r})=\rho_c(\mathbf{r})+\rho_f(\mathbf{r}), \tag{2}$$

where the electron density of the cluster ρ_c is zero outside the volume V, the electron density of the environment ρ_f coincides with ρ_{id} outside the volume V and decreases rapidly to zero inside V. Correspondingly, we can separate the nuclear potential and the electrostatic potential $\varphi(\mathbf{r})$ generated by electrons into contributions from the cluster and environment, i.e.,

$$V(r)=V_c(r)+V_f(r), \tag{3}$$

$$\varphi(\mathbf{r})=\varphi_c(\mathbf{r})+\varphi_f(\mathbf{r}). \tag{4}$$

The main idea of the EDFT method is to ''freeze'' the electron density ρ_f and obtain ρ_c using a set of one-electron orbitals $\psi_i(\mathbf{r})$ localized in the cluster region V,

$$\rho_c(\mathbf{r})=\sum_{i=1}^{N}|\psi_i(\mathbf{r})|^2. \tag{5}$$

Here $\{\psi_i,\ i=1,\ldots,N\}$ are the N lowest energy solutions of the Kohn–Sham equation

$$\left\{-\frac{1}{2}\nabla^2+V_{\mathrm{eff}}[\rho_c,\rho_f]\right\}\psi_i(\mathbf{r})=\epsilon_i\psi_i(\mathbf{r}), \tag{6}$$

where $V_{\mathrm{eff}}[\rho_c,\rho_f]$ is effective potential defined as

$$V_{\mathrm{eff}}[\rho_c,\rho_f]=\frac{\delta}{\delta\rho_c}\{E_{\mathrm{pot}}[\rho_c,\rho_f]+\Delta T_0[\rho_c,\rho_f]\}. \tag{7}$$

The first term in the curly brackets in Eq. (7) is the potential energy

$$E_{\mathrm{pot}}[\rho_c,\rho_f]=E^c_{\mathrm{Coul}}[\rho_c]+E^{c-f}_{\mathrm{Coul}}[\rho_c,\rho_f]+E_{\mathrm{xc}}[\rho_c+\rho_f] \tag{8}$$

which includes the Coulomb energy for the isolated cluster

$$E^c_{\mathrm{Coul}}[\rho_c]=\int d\mathbf{r}\rho_c(\mathbf{r})V_c(\mathbf{r})+\frac{1}{2}\int dr\rho_c(\mathbf{r})\varphi_c(\mathbf{r}), \tag{9}$$

the electrostatic interaction energy between electrons in the cluster with electrons and nuclei in the surrounding

$$E^{c-f}_{\mathrm{Coul}}[\rho_c,\rho_f]=\int d\mathbf{r}\rho_c(\mathbf{r})[V_f(\mathbf{r})+\varphi_f(\mathbf{r})], \tag{10}$$

and the exchange-correlation energy functional $E_{\mathrm{xc}}[\rho_c+\rho_f]$. The second term in the curly brackets in Eq. (7) is called the nonadditive kinetic energy functional whose definition is given by

$$\Delta T_0[\rho_c,\rho_f]=T_0[\rho]-T_0[\rho_c]-T_0[\rho_f], \tag{11}$$

where $T_0[\rho]$ is the kinetic energy functional for a system of independent electrons. Normally, integrations in $E_{\mathrm{xc}}[\rho_c+\rho_f]$ and $\Delta T_0[\rho_c,\rho_f]$ are over all space. However, since ρ_c is nonzero only inside cluster volume V, the result of integration outside V does not depend on ρ_c, thus grid points for computing these integrals can be limited to V, reducing the computational demand. Ignoring the unimportant additive constant due to interactions in the environment region, the total energy is given by

$$E=T^c+\Delta T_0[\rho_c,\rho_f]+E_{\mathrm{pot}}[\rho_c,\rho_f]+E_{\mathrm{nn}}+E_{\mathrm{nf}}, \tag{12}$$

where T^c is the kinetic energy of the cluster, E_{nn} is the repulsion energy of nuclei in the cluster between themselves and with the nuclei in the environment, E_{nf} is the interaction energy between nuclei in the cluster and frozen electron density in the environment. Note that if exact kinetic energy, exchange, and correlation functionals are used, then the embedded DFT approach gives an exact solution for the ground state of nonpolarizable crystal with localized defect.

Since very accurate approximations for the exchange-correlation functional are currently available,[29–31] the main concern in the embedded DFT method is about relatively low accuracy of the kinetic energy functional $T_0[\rho]$ in Eq. (11). Since $\Delta T_0[\rho_c,\rho_f]$ decreases with decreasing overlap between densities ρ_f and ρ_c, an error associated with this term decreases as well. Therefore, for best performance of the EDFT method the boundary of the cluster region V should be chosen so as to minimize the overlap between ρ_f and ρ_c. Favorable conditions for such choice exist in ionic crystals, where the total electron density is well separated into contributions from individual closed shell ions. Cortona applied the EDFT method for studying energetic properties of the alkali halides crystals[23–26] and found very good agreement with experimental data. Wesolowski and Warshel applied this method for studying solvation phenomena, in particular, the interaction of a Li^+ ion with a water molecule.[27,28]

The goal of our study is to extend the EDFT method for defects and adsorption on ionic crystals surfaces. In the first part of this study, we investigated the accuracy of the embedded DFT approach. This is done by calculating the po-

tential curves of the He_2, Ar_2, and X–H_2O (X=frozen density of Li^+, Na^+, K^+, F^- or Cl^-) systems using this approach and comparing to full quantum calculations. It is important to point out that our goal is to assess the accuracy of the embedded DFT as compared to the full quantum DFT calculations, using these chemical systems as prototypes. Thus, the accuracy of the calculated potential curves in comparison with experiment or more accurate theory is of no concern to us here. To achieve our objectives, it is important to perform both embedded and full quantum DFT calculations using the same basis set, exchange-correlation functional and other computational features. We also compared embedded and full quantum DFT results with those obtained by using the simplest MO embedded cluster model with ECP representation for cations and point charge potential for anions. This analysis provides a qualitative understanding of advantages and limitations of the embedded DFT method. The details of the present calculations are presented in Sec. III and the results are summarized in Sec. IV and discussed in Sec. V.

In the second part of this paper (Sec. VI), we construct an embedded DFT cluster model for studying adsorption on ionic crystals and apply this *ab initio* model to calculations of the adsorption energy curves for H_2O/NaCl(001). Conclusions are summarized in Sec. VII.

III. COMPUTATIONAL DETAILS

For He_2, Ar_2, Li^+–H_2O, Na^+–H_2O, and F^-–H_2O potential curves, full DFT calculations were performed at the all-electron level. The following basis sets were used: 311G* for He; 6-31G* for Ar; 6-31G for Li and Na, and 6-311+G* for F. In the cases of Cl^-–H_2O and K^+–H_2O, the core electrons ($1s^2 2s^2 2p^6$) of ions were represented by the Hay–Wadt ECP (Refs. 32, 33) and their valence electrons were treated explicitly in the double zeta basis set. The standard basis set 6-311++G** was used for water interacting with cations, but polarization and diffuse functions on the oxygen atom were omitted in the anion–water calculations. The geometry of the water molecule optimized with the 6-311++G** basis set (R_{OH}=0.956 Å; ∠HOH=105.5°) was fixed in all calculations. Cations are assumed to approach the water molecule from the O atom side along the bisector of the HOH angle in the C_{2v} symmetry, and the distance is measured between the ion and the oxygen atom. Similarly, anions are assumed to approach the water molecule along the OH bond from the H-side, the distance is measured between the ion and the hydrogen atom in this case.

Frozen electron densities of the free He and Ar atoms and Li^+, Na^+, K^+, F^-, Cl^- ions were calculated by the same methods as above and then fitted using linear combinations of several Gaussian functions. The results of the fitting were used in the calculation of the effective potential V_{eff} in Eq. (6) and the total energy [Eq. (12)] in the embedded DFT approach. In this work, we used the local density approximation for $E_{\text{xc}}[\rho]$: X_α functional for exchange[34] and Vosko–Wilk–Nusair (VWN) functional[35] for correlation,

$$E_{\text{xc}}[\rho]=E_x^{X_\alpha}[\rho]+E_c^{\text{VWN}}[\rho]. \tag{13}$$

The nonadditive kinetic energy was computed using two different approximations for the kinetic energy functional: the local Thomas–Fermi (TF) approximation,

$$T_0^{\text{TF}}[\rho]=C\int \rho^{5/3}(\mathbf{r})\,d\mathbf{r} \tag{14}$$

and one of the most accurate nonlocal approximations suggested by Thakkar[36]

$$T_0^{\text{Thakkar}}[\rho]=C\int \rho^{5/3}(\mathbf{r})\left\{1+\frac{0.0055y^2}{1+0.0253y\,\sinh^{-1}y}-\frac{0.072y}{1+2^{5/3}y}\right\}d\mathbf{r}, \tag{15}$$

where

$$y=\frac{|\nabla\rho(\mathbf{r})|}{\rho^{4/3}(\mathbf{r})}$$

and

$$C=\frac{\pi^{4/3}3^{5/3}}{10}.$$

These two approaches are referred to as EDFT-TF and EDFT-Thakkar, respectively and were implemented in our locally modified version of the GAUSSIAN 92/DFT computer code.[37]

In order to calculate binding energies in the EDFT approach, one need to know an energy of the frozen density species separately. Currently, we do not have computational tools to make such calculations. However, we plan to implement this feature in the next version of our computer code. In the present work, we simply added a constant term to the embedded DFT potential energy curves to coincide with the full DFT curves at some reference distance which was chosen large enough (3.6 Å and 5.6 Å for the He and Ar dimers, respectively, and 5.2 Å for ''ion–water'' systems) to ensure that EDFT and full DFT interaction energies are almost equal at this distance. In fact, additional testing showed that this procedure results in errors less than 0.1 kcal/mol and 1 kcal/mol for binding energies in rare gas dimers and ion–water complexes, respectively. This accuracy is sufficient for our initial qualitative investigation on the feasibility of the EDFT method. Fitting of electron densities to the linear superposition of Gaussian functions was also found to introduce a negligible error.

In the whole-ion pseudopotential calculations of the cation–water complexes, we used ECP suggested in Ref. 38 for Li^+ and Hay–Wadt pseudopotentials[32] for Na^+ and K^+.

IV. RESULTS

In this section we present results of full quantum, whole-ion pseudopotential and embedded DFT calculations for helium and argon dimers and complexes of Li^+, Na^+, K^+, F^-, and Cl^- ions with water. In studying the rare gas dimers, we focus on comparison of our results with Gordon–Kim calculations.[39] The kinetic and potential energy contributions to the total binding energy are analyzed in greater details in

TABLE I. Binding energies (in kcal/mol) of He_2, Ar_2, and ion–water complexes.

	E_{full} (this work)	$E_{WIP}-E_{full}$[a]	$E_{EDFT}-E_{full}$ TF	$E_{EDFT}-E_{full}$ Thakkar	E_{full} Ref. 40
He_2	0.3		−0.2	+0.6	
Ar_2	1.0		−0.4	+1.5	
Li^+/H_2O	38	−10	+4	+5	35.46
Na^+/H_2O	29	−6	−2	−7	24.21
K^+/H_2O	21	−2	+1	+8	16.97
F^-/H_2O	33		−7	−7	24.45[b]
Cl^-/H_2O	27		−11	−9	12.42[c]

[a]WIP=whole-ion pseudopotential calculation.
[b]The angle between the C_{2v} axis of the water molecule and the F–O axis is 47.9°.
[c]The angle between the C_{2v} axis of the water molecule and the Cl–O axis is 37.8°.

the case of the Ar dimer. The Li^+-H_2O system is used for discussion of the electron density redistribution in the complex. We discuss the ''electron leak'' problem and polarization effects using the $Cl^-–H_2O$ complex as an example. Results for the ion–water complexes will be utilized in Sec. VI where embedded DFT cluster model for H_2O adsorption on the NaCl(001) surface is considered.

Potential energy curves from the full, embedded DFT and whole-ion pseudopotential calculations are presented in Figs. 1, 2, 5, and 7–10. Table I contains approximate binding energies derived from these curves as well as accurate values calculated by Clementi and co-workers.[40]

A. Helium dimer

The Gordon–Kim method[39] can be considered as a particular case of the embedded DFT method in which both cluster and environment electron densities are fixed. The Gordon–Kim approach gives remarkably good results when applied to interactions between closed shell systems such as rare gas atoms. Therefore, a good agreement between our EDFT-TF and full DFT potential energy curves for the He_2 molecule with that obtained by Gordon and Kim[39] is not surprising (see Fig. 1). However, the EDFT-Thakkar method gives worst agreement; the binding energy is overestimated by about 0.6 kcal/mol and the equilibrium distance is too short by about 0.5 Å compared to the full DFT results.

B. Argon dimer

Results obtained for the argon dimer (see Fig. 2) are qualitatively similar to those reported above for He_2. The EDFT-TF potential energy curve lies between full DFT and Gordon–Kim results, as expected. The EDFT-Thakkar method overestimates the strength of chemical bond in Ar_2. For better understanding of the performance of the EDFT approach, we analyzed separate contributions to the total energy curves from the kinetic and potential energy terms. This analysis is presented in Fig. 3 where we plot errors (deviations with respect to full DFT results) characteristic for EDFT-TF, EDFT-Thakkar, and Gordon–Kim levels of the embedded DFT theory. First note that, although, there are large errors in description of both kinetic and potential energy of the molecule (about 6, 60, and 14 kcal/mol for these three methods, respectively, at internuclear separation greater than 3 Å), the total energy (sum of the kinetic and potential energies) is represented rather accurately (the errors do not exceed 2.5 kcal/mol). This cancellation of errors can be understood by applying arguments first suggested by Harris[41]: in the vicinity of the actual electron density distribution, the total energy of the molecule has a weak quadratic dependence on the variations of the density. Therefore, even for approximate total densities used in the EDFT approach, calculations of the total energy may be quite accurate. Note also that errors associated with the ''half-frozen'' EDFT-TF approach are smaller than those for the ''fully-frozen'' Gordon–Kim method, as expected. The origin of large errors in the EDFT-Thakkar approach are not clear yet (see also Sec. V).

Additional evidence on the accuracy of the EDFT method is presented in Fig. 4 where we compare contributions to the binding energy from the nonadditive kinetic energy, exchange, and correlation energies calculated with full DFT, Gordon–Kim, and EDFT-TF method. Exchange and

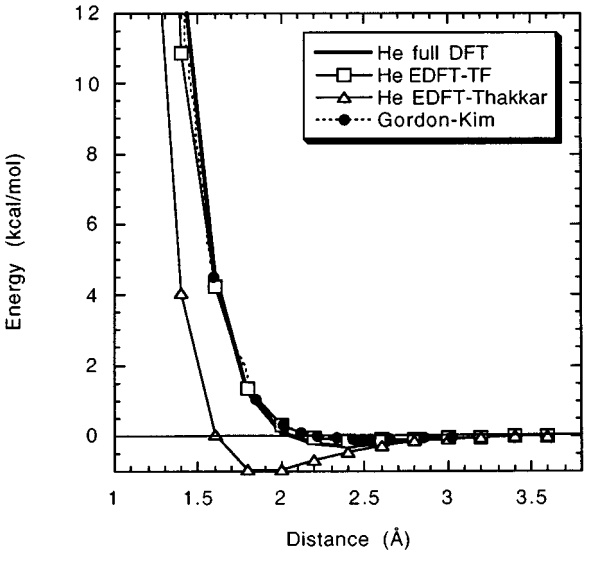

FIG. 1. Potential energy curves for the He dimer.

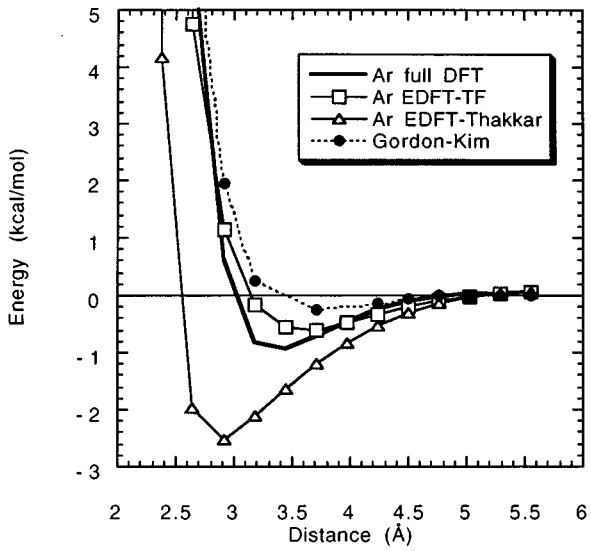

FIG. 2. Potential energy curves for the Ar dimer.

correlation contributions facilitate binding, while the nonadditive kinetic energy leads to repulsion of two argon atoms. All terms decay exponentially with increasing the Ar–Ar distance. Note also a good correspondence between our TF-EDFT results and those from Gordon–Kim calculations.

C. $Li^+\cdots H_2O$

Both EDFT-TF and EDFT-Thakkar calculations overestimate the binding energy by 4–5 kcal/mol and slightly underestimate the short-range repulsion between Li^+ and water (see Fig. 5). In the opposite, the binding energy is too low in the whole-ion pseudopotential approach.

A more detailed picture of the performance of the EDFT-TF method can be seen in Fig. 6. where we plot the difference $\Delta\rho$ between the total electron density in the Li^+–H_2O complex at the equilibrium separation of 1.8 Å and

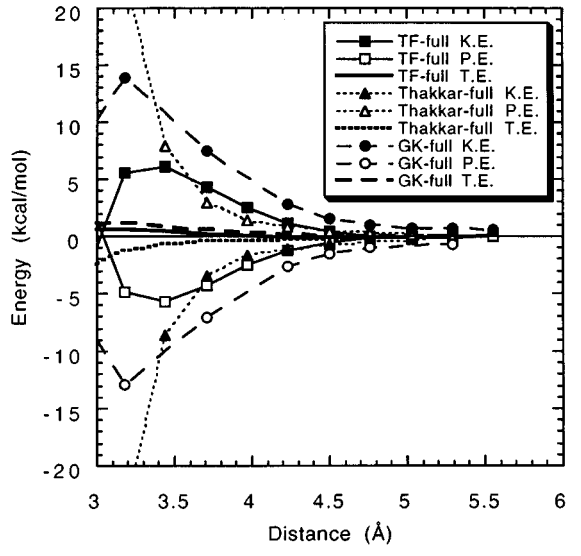

FIG. 3. Differences between various EDFT energies and those from full DFT calculations for the Ar dimer. Full lines and squares refer to the EDFT-TF method, dotted lines and triangles are for the EDFT-Thakkar method, dashed lines and circles are for the Gordon–Kim method (Ref. 39). Results for total energy differences are shown by thick lines, while those for kinetic and potential energy differences are marked by filled and empty symbols, respectively.

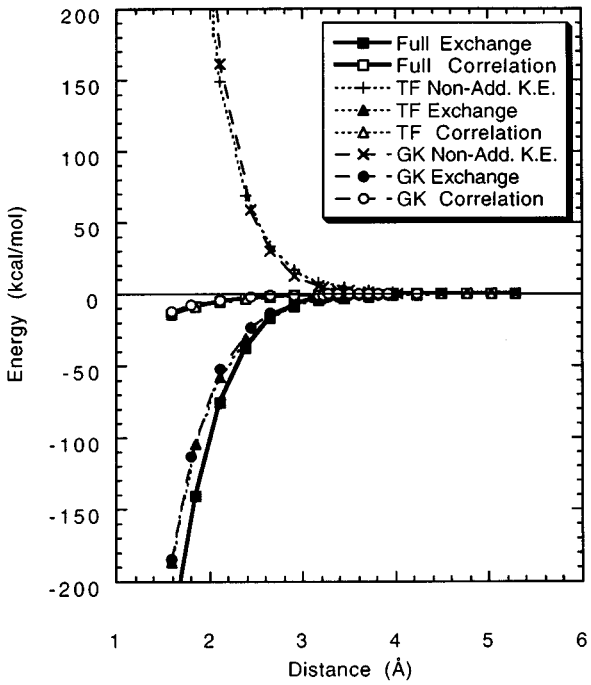

FIG. 4. Nonadditive kinetic energy (crosses), exchange (filled symbols), and correlation (empty symbols) contributions to the binding energy of the Ar dimer calculated with the full DFT (thick solid lines), EDFT-TF (dotted lines), and Gordon–Kim (dashed lines) methods.

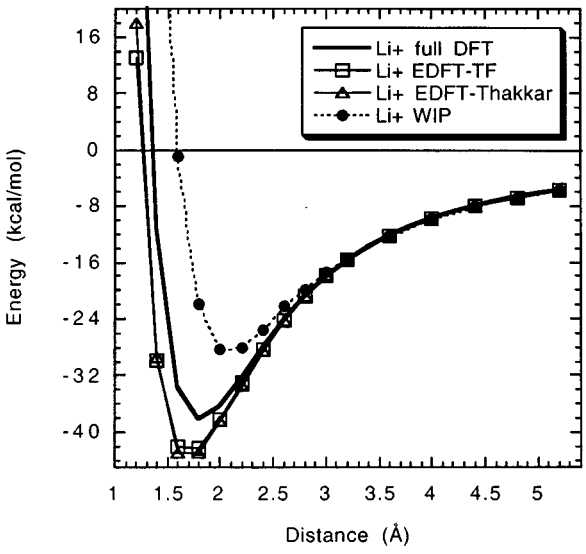

FIG. 5. Potential energy curves for the Li^+–H_2O complex.

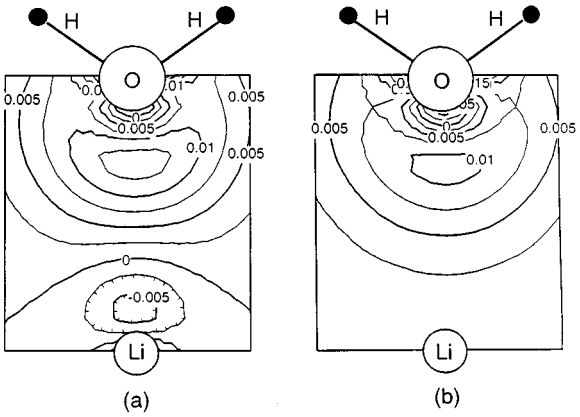

FIG. 6. The differential electron density for the Li^+–H_2O complex. (a) Full DFT calculation; (b) EDFT-TF calculation. Isodensity values are in e/bohr^3.

the sum of densities of the free water molecule and the Li^+ ion. Positive values of the differential electron density $\Delta\rho$ near the oxygen atom of water correspond to the attraction of the water electron density to the positive charge of Li^+. This part of the electron density redistribution is reproduced fairly well by the embedded DFT method. On the other hand, $\Delta\rho$ from the full DFT calculation shows a substantial polarization of the Li^+ ion induced by the repulsive potential from the negatively charged oxygen atom of water. Such an induced polarization effect is neglected in the embedded DFT method.

Note that in the previous work by Wesolowski and Warshel,[27,28] the authors found large discrepancies between the full DFT and EDFT-TF results for this system. Using a theoretically similar approach, we did not find such discrepancies here. Discrepancies found by Wesolowski and Warshel are mainly due to their implementation of the EDFT theory, in particular, basis set effects and numerical integration scheme.[42] Recent implementation of the EDFT method by Wesolowski and Weber[43] yields results in good agreement with ours.

D. $Na^+\cdots H_2O$

The EDFT-TF method underestimates the Na^+–H_2O binding energy by about 2 kcal/mol with respect to the results from the full DFT calculation (see Fig. 7). Both EDFT-Thakkar and whole-ion pseudopotential methods give even lower binding energies.

E. $F^-\cdots H_2O$

The EDFT-TF results (Fig. 8) have some peculiar features: at distances shorter than 1.4 Å, there is a rapid decrease in energy instead of a strong repulsion. A detailed analysis of the electronic structure at these short distances showed that there is an unphysical redistribution of the electron density of the water molecule to the core region of the F^- ion. Apparently, there is an attractive electrostatic potential which acts on the electron density in the vicinity of the fluorine nucleus. In the full DFT calculations, this attraction

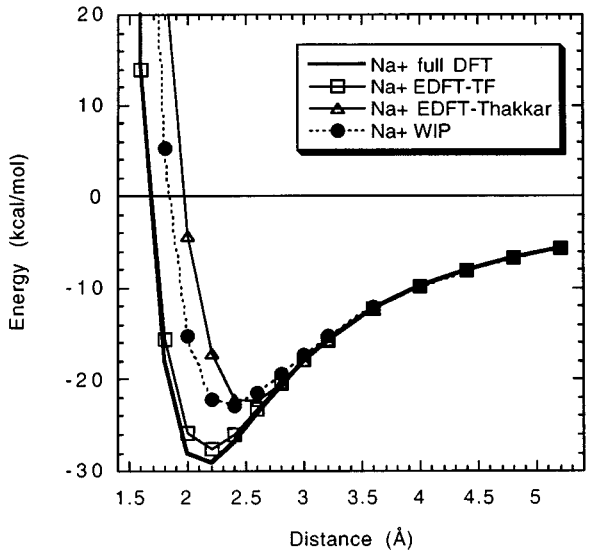

FIG. 7. Potential energy curves for the Na^+–H_2O complex.

is compensated by the Pauli repulsion with the core electrons of F^- forbidding the water electrons to penetrate into this region of space. Our results indicate that the approximate nature of the nonadditive kinetic energy functional in the embedded DFT approach cannot properly take into account this repulsion, consequently, it results in the unphysical "electron leak."

To deal with this problem we suggested to use a hybrid EDFT-ECP method. In this approach, the core 1s electrons of the F^- ion are represented by the Stevens–Basch–Krauss effective core pseudopotential[44] and the valence electrons of the F^- ion are treated in the embedded DFT formalism. The valence electron density of F^- for this purpose was computed using the CEP-311+G basis set. The EDFT-TF/ECP

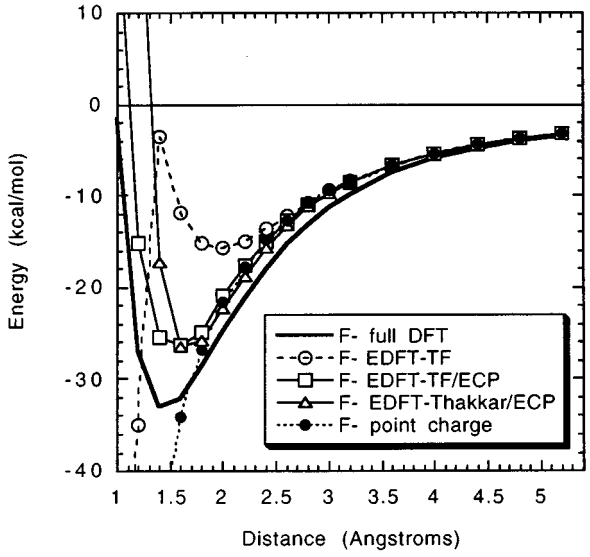

FIG. 8. Potential energy curves for the F^-–H_2O complex.

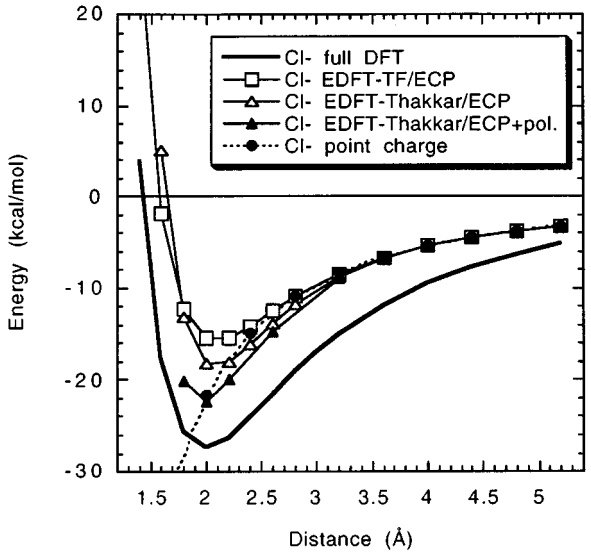

FIG. 9. Potential energy curves for the Cl^-–H_2O complex.

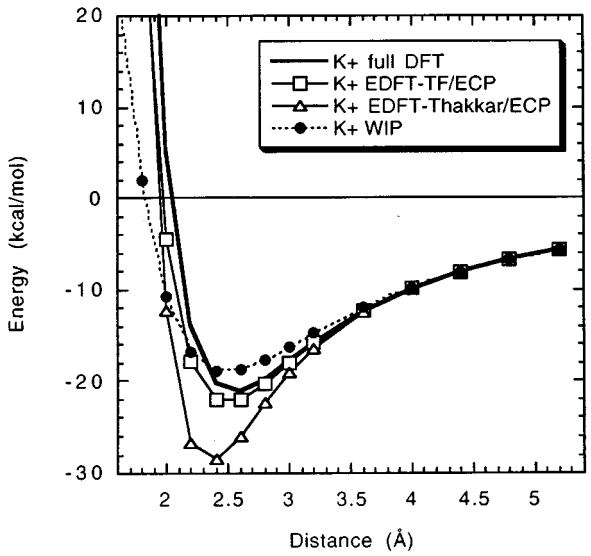

FIG. 10. Potential energy curves for the K^+–H_2O complex.

and EDFT-Thakkar/ECP potential energy curves are shown in Fig. 8. Clearly, these approaches reproduce qualitatively the ion–water repulsion, however, the binding energies are too small by about 7 kcal/mol compared to the full DFT result.

F. $Cl^-\cdots H_2O$

This case provides another dramatic example for the failure of the straightforward embedded DFT approach, when using the frozen *total* electron density for Cl^-. The electron leak to the Cl^- core region and an abrupt decrease of the total energy, similar to that in the F^-–H_2O system, starts to occur when the Cl–H distance is about 5 Å. However, the hybrid EDFT/ECP method with the use of the Hay–Wadt pseudopotential[32] for Cl^- core electrons ($1s^2 2s^2 2p^6$) and frozen valence electron density computed with the double-zeta basis set allows us to obtain qualitatively reasonable results for the Cl^-–H_2O interaction curve (Fig. 9). Similar to the F^-–H_2O system, the binding energies are too small by 9–11 kcal/mol as compared with the full DFT result.

One of the reasons for the discrepancies between embedded and full DFT results for both the F^-–H_2O and Cl^-–H_2O is the induced polarization of the anions in the electric field of the polar water molecule that is neglected in the embedded DFT approach. To illustrate and estimate the magnitude of the polarization contribution, we recalculated several points on the EDFT-Thakkar/ECP potential energy curve using a simple model to represent the polarizable valence electron density of Cl^-. This approximate method resembles the semiempirical ''shell model'' used for classical atomistic simulations of ionic crystals.[45] The idea of our method is to model the polarizability of the Cl^- valence electrons as a rigid displacement of the valence electron density with respect to the position of the core. The only parameter of our ''shell model'' is the force constant k specifying a harmonic potential of the form kr^2 between the core and the center of the frozen valence electron density distribution. This force constant k was fitted to reproduce the polarizability of the free Cl^- ion (31 a.u.) (Ref. 46) and has a value of 0.793 a.u.

By using the method outlined above, we optimized position of the electron shell at each selected Cl core–water distance. The calculated energies are shown in Fig. 9 as filled triangles. Apparently, the electron polarization of the Cl^- ion starts to contribute significantly to the Cl^-–H_2O interaction energy at distances smaller than 3 Å and the binding energy of the Cl^-–H_2O complex increases by about 5 kcal/mol in better agreement with the full DFT calculations.

Another effect contributing to the binding energies of anion–water complexes is the charge transfer: at the equilibrium distance of 2 Å there is about 0.2 electrons transferred from Cl^- to H_2O according to the Mulliken population analysis of the full DFT results. This charge transfer may be responsible for several kcal/mol attractive interaction which is not taken into account in the embedded DFT calculations.

G. $K^+\cdots H_2O$

As in the cases of F^-–H_2O and Cl^-–H_2O, we performed a hybrid EDFT/ECP study for the K^+–H_2O system. Similarly to the cases of Li^+ and Na^+ the best EDFT/ECP results were obtained with the use of the TF functional (see Fig. 10). The EDFT-Thakkar/ECP binding energy is too large by about 8 kcal/mol. The whole-ion pseudopotential representation of the total K^+ electron density yields too small binding energy and soft repulsive potential at small distances.

V. DISCUSSION OF THE GAS PHASE CALCULATIONS

First note that our full DFT calculations strongly overestimate the binding energies of the studied systems, especially in the case of Cl^-–H_2O (see Table I). This is a result of using the local density approximation for the exchange-correlation

functional.[47] As discussed in Sec. II, these errors are not very important for our comparison of different approximate DFT models.

EDFT-TF results for the ion–water complexes are in better agreement with the full DFT calculations than those obtained in the whole-ion pseudopotential approach. This is particularly encouraging. However, there are still three major sources of errors in the embedded DFT calculations; (i) neglect of the electron density redistribution in the frozen density species; (ii) difficulties with ensuring the N-representability of the cluster electron density ρ_c; and (iii) an approximate form of the kinetic energy functional used in the calculation of the nonadditive kinetic energy term [Eq. (11)]. The first effect is clearly demonstrated in our ''shell model'' calculations for the Cl^-–H_2O complex. This simple approximation for the polarization of the ρ_f improves the accuracy of the embedded DFT model substantially. Using more realistic polarizable densities may also help to avoid errors from the second source (ii). These errors appear from the fact that for accurate implementation of the EDFT method, the frozen part of the electron density ρ_f should be chosen so that ρ_c satisfies the N-representability conditions. In particular, ρ_c should be non-negative, differentiable and its integral over volume V should be an integer number.[48] However, it is often difficult to ensure the former condition because ρ_c is not known *a priori*. As shown in Fig. 6, freezing the free ion density of Li^+ in calculations of the Li^+–water complex violates this condition: the differential electron density from the full DFT calculation is negative close to the Li nucleus. Therefore, for correct description of the total electron density, ρ_c should be negative in some region space, but it is impossible when the representation given in Eq. (5) is used for ρ_c. This inconsistency introduces a certain error in the EDFT calculated properties which can be reduced by using a polarizable density of Li^+ or by decreasing ρ_f in the regions of space where negative differential electron density is expected. The latter method implies that any redistribution of the electron density in the frozen part can be effectively taken into account by using sufficiently large and diffuse basis set in the cluster. However, this is true only if the nonadditive kinetic energy functional is accurate enough to deal with large overlap of the electron densities in the cluster and surrounding. Therefore, the low accuracy of existing kinetic energy functionals is the principal factor limiting the quality and applicability of the embedded DFT method. Deficiencies of the current kinetic energy functionals are clearly seen in our results for the F^-–H_2O and Cl^-–H_2O complexes where we needed to reduce effectively ρ_f and its overlap with ρ_c by using the effective core pseudopotential approximation for anions in order to avoid unphysical results.

The embedded DFT method with the local TF kinetic energy functional was found to give more accurate results than with the nonlocal Thakkar functional. A similar effect was found by Lacks and Gordon[49] in their calculations of the interaction kinetic energy for rare gas dimers: nonlocal gradient corrected functionals are not necessarily more accurate than the Thomas–Fermi one for this particular property. This is surprising because the Thakkar functional yields much better results for total kinetic energies of atoms and molecules than the TF functional. For instance, the mean error for a set of 77 molecules was found to be 0.15% and 8.57% for these two functionals, respectively.[36] Obviously, the relative performance of different kinetic energy functionals requires further study. As more accurate approximations for T_0 becoming available, the accuracy of the embedded DFT model will be improved and its applications to a broader range of systems will be possible.

VI. EMBEDDED DFT CLUSTER MODEL FOR CALCULATION OF WATER ADSORPTION ON THE NaCl(001) SURFACE

To illustrate how the embedded DFT method can be used to study adsorption, we have carried out EDFT-TF calculations for the adsorption of H_2O on the NaCl(001) surface. This system is important for atmospheric chemistry.[50] In fact, interaction of water molecules with the surface of ionic crystals has been a subject of theoretical studies for many years. Barraclough and Hall[51] formulated a simple classical potential model for the H_2O/NaCl(001) adsorption in which H_2O was considered as a point particle with a fixed dipole moment, polarizability, and repulsion constant. A similar polarizable electropole model was used in Ref. 52 for molecular dynamics studies of two-dimensional ordering of the H_2O layer on NaCl(001). A more realistic model, where the water–surface interaction potential was built as a superposition of ion–water potentials fitted to results of *ab initio* calculations by Clementi and co-workers[40] was also available.[53,54]

These simplistic classical models can not properly take into account important quantum effects such as the redistribution of electron densities of both adsorbate and substrate and formation of hydrogen bonds. These effects play an important role in mechanisms of chemical reactions and chemisorption of water at defect sites on the surface of alkali halide crystals.[50,55] Application of quantum semiempirical[56,57] and model Hamiltonian[58] methods to these systems has a limited predictive value due to the presence of parameters that were fitted to particular experimental data. In view of these facts, it is interesting to develop a fully *ab initio* quantum mechanical model for the H_2O/NaCl adsoption.

The EDFT-TF cluster considered in this study consisted of the water molecule and nine-atom 3×3 square cluster $[Na_5Cl_4]^+$ on the surface (see Fig. 11). All first neighbors of these nine atoms in the lattice were modelled as frozen density Na^+ and Cl^- ions: ρ_f was approximated as a sum of densities of individual ions which were taken from the gas phase calculations above. The lattice ions lying beyond the first coordination sphere were treated approximately as point charges occupying ideal positions in the $8\times8\times4$ block of the crystalline lattice. In our previous study,[16] we have shown that this model generates the electrostatic potential very close to the exact Madelung potential on the (001) surface of fcc crystals.

The internal geometry of the water molecule was fixed while approaching the surface in three different orientations

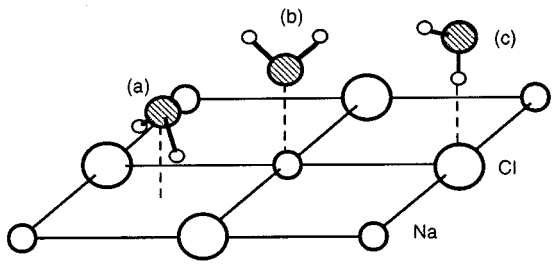

FIG. 11. Cluster $[Na_5Cl_4]^+$ on the (001) surface of NaCl and different orientations of the adsorbed water molecule. (a) Above the middle of the square Na_2Cl_2; (b) above a Na^+ cation; (c) above a Cl^- anion.

as shown in Fig. 11. In agreement with the previous report,[53] we did not find stable adsorption of water above the middle of the surface Na_2Cl_2 square [Fig. 11(a)]. The potential energy curves for adsorption above Na^+ and Cl^- are shown in Fig. 12. Calculated data were fitted to a Morse function. The plotted distances in these two cases are Na^+–O and Cl^-–H, respectively. Adsorption energy of about 9 kcal/mol was obtained for adsorption above the Na^+ ion [Fig. 11(b)]. This finding is also in agreement with previous classical calculations.[51,53] Our calculations predict adsorption energy of about 9 kcal/mol for the ''single hydrogen bond'' adsorption above Cl^- [Fig. 11(c)]. This result disagrees with the classical calculations[51,53] which predict much weaker attraction to the anions. This, however, is expected since the full DFT binding energy of the Cl^-–H_2O complex is also too large. As we pointed out in Sec. V, this discrepancy is a result of using the local density approximation in our calculations.

VII. CONCLUSIONS

We have demonstrated that the embedded density functional formalism can be successfully implemented for studying defects and adsorption in crystals and solvation complexes as an alternative to existing molecular orbital embedded cluster models. For heavy polarizable ions, this approach should be supplemented with the pseudopotential description of the core electrons and model representation of the polarizability. The simple and accurate treatment of the correlation between electrons in the cluster and surrounding seems to be the main advantage of the embedded DFT method. Moreover, the frozen electron density in the environment required for embedded DFT calculations can be easily obtained from routine band structure calculations. Determination of pseudopotentials or model potentials required for MO embedded cluster studies is more difficult, especially in the case of nonspherical ions. Although at the present stage both the embedded DFT and MO cluster approaches seem to be limited to the systems in which electron densities of fragments are well separated, such as ionic crystals, the basic approximations of these two approaches are rather different and full comparison of their relative performance and applicability requires further studies.

Further improvements of the present embedded DFT cluster model include (i) using of more accurate nonlocal exchange-correlation functionals; (ii) self-consistent optimizing of electron densities for ions in crystal; (iii) taking into account the polarization of the lattice by the adsorbate; and (iv) developing the EDFT methodology for systems with covalent and ionic–covalent bonding, such as metal oxides. These steps are currently underway in our lab. However, the most crucial factor determining the accuracy of the embedded DFT approach is the accuracy of the kinetic energy functional. Research in this area is making rapid progress. Thus, a considerable improvement of the embedded DFT approach and its applications to a wider class of chemical systems are hopeful.

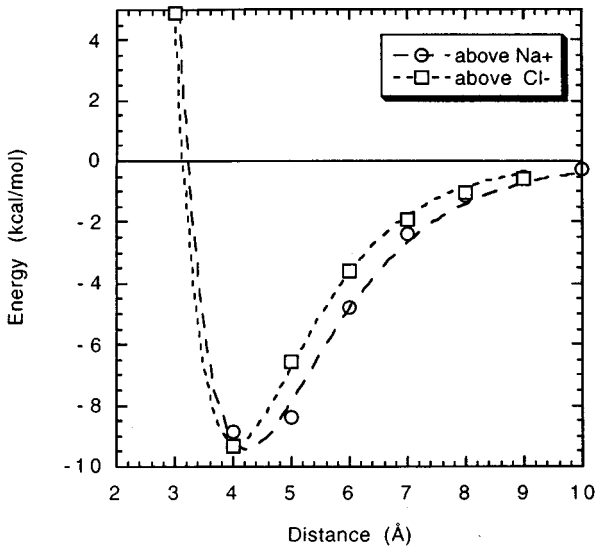

FIG. 12. Potential energy curves for H_2O adsorption on the NaCl(001) surface.

ACKNOWLEDGMENTS

This work was supported by the University of Utah and the National Science Foundation through a NSF Young Investigator Award to T.N.T. Authors wish to thank Professor A.L. Shluger for stimulating discussions and Dr. T. Wesolowski for sending his manuscript prior to publication.

[1] S. T. Pantelides, Rev. Mod. Phys. **150**, 797 (1978).
[2] C. Pisani, R. Dovesi, R. Nada, and L. Kantorovich, J. Chem. Phys. **92**, 7448 (1990).
[3] L. N. Kantorovich, J. Phys. C **21**, 5041 (1988).
[4] J. M. Vail, J. Phys. Chem. Solids **51**, 589 (1990).
[5] Z. Barandiarán and L. Seijo, in *Computational Chemistry: Structure, Interactions and Reactivity*, edited by S. Fraga (Elsevier, New York, 1992), Vol. 77(B), p. 435.
[6] W. C. Nieuwpoort and R. Broer, in *Cluster Models for Surface and Bulk Phenomena*, edited by G. Pacchioni (Plenum, New York, 1992), p. 505.
[7] R. McWeeny and B. T. Sutcliffe, *Methods of Molecular Quantum Mechanics* (Academic, London, 1969).
[8] S. Huzinaga and A. A. Cantu, J. Chem. Phys. **55**, 5543 (1971).
[9] S. Huzinaga, D. McWilliams, and A. A. Cantu, Adv. Quantum Chem. **7**, 187 (1973).

[10] N. W. Winter, R. M. Pitzer, and D. K. Temple, J. Chem. Phys. **87**, 2945 (1987).
[11] N. W. Winter, R. M. Pitzer, and D. K. Temple, J. Chem. Phys. **86**, 3549 (1987).
[12] R. L. Martin, in *Cluster Models for Surface and Bulk Phenomena*, edited by G. Pacchioni (Plenum, New York, 1992), p. 485.
[13] V. E. Puchin, A. L. Shluger, K. Tanimura, and N. Itoh, Phys. Rev. B **47**, 6226 (1993).
[14] V. E. Puchin, A. L. Shluger, and N. Itoh, Phys. Rev. B **47**, 10 760 (1993).
[15] V. E. Puchin, A. L. Shluger, Y. Nakai, and N. Itoh, Phys. Rev. B **49**, 11 364 (1994).
[16] E. V. Stefanovich and T. N. Truong, J. Chem. Phys. **102**, 5071 (1994).
[17] J. L. Pascual, L. Seijo, and Z. Barandiarán, J. Chem. Phys. **98**, 9715 (1993).
[18] Z. Barandiarán and L. Seijo, in *Cluster Models for Surface and Bulk Phenomena*, edited by G. Pacchioni (Plenum, New York, 1992), p. 565.
[19] L. N. Kantorovich and B. P. Zapol, J. Chem. Phys. **96**, 8420 (1992).
[20] D. E. Ellis, G. A. Benesh, and E. Byrom, Phys. Rev. B **16**, 3308 (1977).
[21] D. E. Ellis, J. Guo, and D. J. Lam, J. Am. Ceram. Soc. **73**, 3231 (1990).
[22] J. Guo, D. E. Ellis, and D. J. Lam, Phys. Rev. B **45**, 3204 (1992).
[23] P. Cortona, Phys. Rev. B **44**, 8454 (1991).
[24] P. Cortona, Phys. Rev. B **46**, 2008 (1992).
[25] P. Cortona, Nuovo Cimento D **15**, 243 (1993).
[26] P. Cortona and A. V. Monteleone, Int. J. Quantum Chem. **52**, 987 (1994).
[27] T. Wesolowski and A. Warshel, J. Phys. Chem. **97**, 8050 (1993).
[28] T. Wesolowski and A. Warshel, J. Phys. Chem. **98**, 5183 (1994).
[29] A. D. Becke, J. Chem. Phys. **98**, 1372 (1993).
[30] A. D. Becke, J. Chem. Phys. **98**, 5648 (1993).
[31] C. Lee, W. Yang, and R. G. Parr, Phys. Rev. B **37**, 785 (1988).
[32] P. J. Hay and W. R. Wadt, J. Chem. Phys. **82**, 284 (1985).
[33] P. J. Hay and W. R. Wadt, J. Chem. Phys. **82**, 299 (1985).
[34] J. C. Slater, *Quantum Theory of Molecules and Solids* (McGraw-Hill, New York, 1974), Vol. 4.
[35] S. H. Vosko, L. Wilk, and M. Nusair, Can. J. Phys. **58**, 1200 (1980).
[36] A. J. Thakkar, Phys. Rev. A **46**, 6920 (1992).
[37] GAUSSIAN 92/DFT, Revision G.3, M. J. Frisch, G. W. Trucks, H. B. Schlegel, P. M. W. Gill, B. G. Johnson, M. W. Wong, J. B. Foresman, M. A. Robb, M. Head-Gordon, E. S. Replogle, R. Gomperts, J. L. Andres, K. Raghavachari, J. S. Binkley, C. Gonzalez, R. L. Martin, D. J. Fox, D. J. Defrees, J. Baker, J. J. P. Stewart, and J. A. Pople (Gaussian, Inc., Pittsburgh, PA, 1993).
[38] J. C. Barthelat, P. Durand, and A. Serafini, Mol. Phys. **33**, 159 (1977).
[39] R. G. Gordon and Y. S. Kim, J. Chem. Phys. **56**, 3122 (1972).
[40] H. Kistenmacher, H. Popkie, and E. Clementi, J. Chem. Phys. **59**, 5842 (1973).
[41] J. Harris, Phys. Rev. B **31**, 1770 (1985).
[42] T. W. Wesolowski (private communication).
[43] T. W. Wesolowski and J. Weber, Chem. Phys. Lett. (in press).
[44] W. Stevens, H. Basch, and J. Krauss, J. Chem. Phys. **81**, 6026 (1984).
[45] B. G. Dick and A. W. Overhauser, Phys. Rev. **112**, 90 (1958).
[46] A. K. Das, D. Ray, and P. K. Mukherjee, Theor. Chim. Acta **82**, 223 (1992).
[47] B. G. Johnson, P. M. W. Gill, and J. A. Pople, J. Chem. Phys. **98**, 5612 (1993).
[48] R. G. Parr and W. Yang, *Density-Functional Theory of Atoms and Molecules* (Oxford University, New York, 1989).
[49] D. J. Lacks and R. G. Gordon, J. Chem. Phys. **100**, 4446 (1994).
[50] D. J. Dai, S. J. Peters, and G. E. Ewing, J. Phys. Chem. **99**, 10 299 (1995).
[51] P. B. Barraclough and P. G. Hall, Surf. Sci. **46**, 393 (1974).
[52] B. Wassermann, S. Mirbt, J. Reif, J. C. Zink, and E. Matthias, J. Chem. Phys. **98**, 10049 (1993).
[53] T. V. Egorova, L. N. Kantorovich, A. I. Livshits, and A. L. Shluger, Russ. J. Phys. Chem. **55**, 760 (1981).
[54] N. Anastasiou, D. Fincham, and K. Singer, J. Chem. Soc. Faraday Trans. II **79**, 1639 (1983).
[55] S. Fölsch and M. Henzler, Surf. Sci. **247**, 269 (1991).
[56] L. N. Kantorovich and A. L. Shluger, Khim. Fiz. **10**, 2277 (1984).
[57] E. V. Stefanovich, A. L. Shluger, and Y. E. Tiliks, Khim. Fiz. **7**, 815 (1988).
[58] E. N. Korol and O. Y. Posudievsky, Surf. Sci. **169**, 104 (1986).